Environ. Sci. Technol. **2004**, *38,* 555−569

Global Source Attribution for Mercury Deposition in the United States

CHRISTIAN SEIGNEUR,*,† KRISH VIJAYARAGHAVAN,† KRISTEN LOHMAN,† PRAKASH KARAMCHANDANI,† AND COURTNEY SCOTT‡

Atmospheric & Environmental Research, Inc., Suite 120, 2682 Bishop Drive, San Ramon, California 94583, and Atmospheric & Environmental Research, Inc., 131 Hartwell Avenue, Lexington, Massachusetts 02421

A multiscale modeling system that consists of a global chemical transport model (CTM) and a nested continental CTM was used to simulate the global atmospheric fate and transport of mercury and its deposition over the contiguous United States. The performance of the CTMs was evaluated against available data. The coefficient of determination (r^2) for observed versus simulated annual mercury wet deposition fluxes over North America was 0.50 with average normalized error and bias of 25% and 11%, respectively. The CTMs were used to conduct a global source attribution for selected receptor areas. Three global emission scenarios were used that differed in their distribution of background emissions among direct natural emissions and re-emissions of natural and anthropogenic mercury. North American anthropogenic sources were calculated to contribute only from 25 to 32% to the total mercury deposition over the continental United States. At selected receptors, the contribution of North American anthropogenic emissions ranges from 9 to 81%; Asian anthropogenic emissions were calculated to contribute from 5 to 36%; natural emissions were calculated to contribute from 6 to 59%.

Introduction

The origin of atmospheric mercury that is deposited to watersheds in the United States is currently poorly understood. The relative contributions of local, regional, and global anthropogenic sources as well as natural sources of mercury are likely to vary across the United States, and it is important to characterize them to assess the likely efficacy of future emission control strategies on the atmospheric deposition of mercury. We present here an analysis of source contributions to mercury dry and wet deposition in the contiguous United States. Our analysis is based on the atmospheric fate and transport modeling of mercury using a multiscale modeling system that simulates the global cycling of mercury as well as its fate and transport over North America for an entire year. This modeling system includes a global chemical transport model (CTM) and a continental CTM, TEAM (*1*). Such an approach is desirable because mercury is a global pollutant with an average atmospheric lifetime on the order of a year. Therefore, the upwind boundary concentrations of mercury species are quite influential for modeling the atmospheric fate and transport of mercury at continental and regional scales (*2*). Because there is a paucity of data to specify such boundary conditions, particularly aloft, it is more reliable to obtain such boundary conditions from a global simulation, contingent upon satisfactory performance of the global CTM. Thus, the global CTM provides spatially distributed and temporally resolved fields of background mercury species concentrations, and the continental CTM uses these background concentrations along with the mercury emissions within the continental domain to calculate mercury fate and transport at a spatial resolution finer than that of the global CTM. This modeling system was updated here to reflect the current state of the science and evaluated with available monitoring data before its application to the analysis of source−receptor relationships.

We present first a brief description of the modeling system including the recent updates made to the atmospheric chemical transformations of mercury. Next, we describe the base emission inventory and two alternative inventories used in this study to bound the uncertainties associated with the background emissions (i.e., natural emissions and re-emissions). Then, we evaluate the performance of this modeling system with available data on mercury ambient concentrations and wet deposition fluxes. Finally, the modeling system is used to perform a source attribution of mercury deposition at selected receptors across the United States. Earlier work presented a similar, but more limited, analysis for mercury deposition in New York state (*3*). The present analysis highlights the large variations that occur in the various global source contributions to mercury deposition across the North American continent.

Description of the Modeling System

The modeling system used in this study consists of two nested models: a global CTM that is run until steady state is achieved between emissions of mercury into the atmosphere and deposition to the earth and a continental CTM that is run for one year, 1998 in this study. The atmospheric emissions and chemistry of mercury are the same in both models. Seigneur et al. (*1*) have described this modeling system and its initial application. For this study, the atmospheric chemical mechanism and some other aspects of the model formulation were updated from those used by Seigneur et al. (*1*) as described below.

Atmospheric Chemical Mechanism. The atmospheric chemical mechanism is based on the work of Seigneur et al. (*4*), with updates described by Shia et al. (*5*) and Seigneur et al. (*1*). This mechanism was included in a recent model intercomparison (*6*). It was updated for this study to reflect recent laboratory data on chemical kinetics and thermodynamics. Those updates are the following.

The gas-phase reaction of Hg(0) with OH radicals was added (*7*). The product was assumed to be $Hg(OH)_2$. The kinetic rate constant is 8×10^{-14} cm^3 molecule^{-1} s^{-1}. The thermodynamic equilibrium constants for the formation of the complexes $HgSO_3$ and $Hg(SO_3)_2^{2-}$ in the aqueous phase were updated on the basis of the work of van Loon et al. (*8*). The kinetics of the gas-phase reaction of Hg(0) with Cl_2 was updated on the basis of the recent laboratory data of Ariya et al. (*9*).

* Corresponding author phone: (925)244-7121; fax: (925)244-7129; e-mail: seigneur@aer.com.
† Atmospheric & Environmental Research, Inc., San Ramon, CA.
‡ Atmospheric & Environmental Research, Inc., Lexington, MA.

10.1021/es034109t CCC: $27.50
Published on Web 12/03/2003

The products of the gas-phase reactions vary among HgO, $Hg(OH)_2$, and $HgCl_2$. HgO can be in the gas phase or the particulate phase because its saturation vapor pressure is low, 9×10^{-17} atm at 25 °C (*10*). For an ozone concentration of 40 ppb, it takes ~4.5 h to convert enough Hg(0) to reach the HgO saturation vapor pressure. HgO is very soluble in water, with a Henry's law constant of 2.69×10^{12} M atm^{-1} at 25 °C (*10*), and HgO particles are likely to be very efficiently scavenged by cloud droplets. Thus, in the presence of clouds, HgO is nearly totally present in the aqueous phase, where it rapidly dissociates to Hg^{2+} (*11*). Then, Hg^{2+} reacts with Cl^-, OH^-, and SO_3^{2-} to form new species. $HgCl_2$ and $Hg(OH)_2$ have saturation vapor pressures that exceed their atmospheric concentrations and consequently do not condense to the particulate phase. Both $HgCl_2$ and $Hg(OH)_2$ are quite soluble and partition between the gas phase and the aqueous phase in the presence of clouds. Therefore, it is not necessary to specify the end products of the oxidation reactions of Hg(0) in the chemical kinetic mechanism because, in the presence of clouds, these species dissolve in cloud droplets where the chemical speciation of Hg(II) is governed by aqueous-phase and gas/droplet equilibria.

Some aqueous-phase equilibria are neglected in this chemical mechanism. Those include the equilibria leading to the formation of $HgCl^+$, $HgCl_3^-$, $HgCl_4^-$, HgOHCl, and $HgOH^+$. Among the various mercury chloride salts, $HgCl_2$ dominates at pH values typical of clouds. Other species may dominate in aqueous particles where pH values can be very low, but atmospheric chemical reactions in aerosols do not contribute significantly on global and regional scales to the total mercury mass budget because of the low liquid water content of particles; atmospheric particles may, however, affect the chemical speciation of mercury in specific cases such as the influence of sea-salt particles in the marine boundary layer (*12*). Therefore, only $HgCl_2$ is relevant to mercury aqueous chemistry for regional/global scales, and it is appropriate here to neglect the other chloride species. Under most conditions, the equilibria favor $HgCl_2$ over $Hg(OH)_2$ and other mercury hydroxide species. These latter species become important only when HCl concentrations become very low. A background HCl surface concentration of 0.7 $\mu g/m^3$ (*13*) is used in the global CTM and in TEAM and, therefore, the mercury hydroxide species can be neglected. $Hg(OH)_2$ is included in the mechanism for sensitivity simulations where HCl concentrations are selected to be very low or even zero.

Global Mercury Chemical Transport Model. The formulation of the global Hg model has been described in detail elsewhere (*1*, *5*). We present here an overview and highlight the recent changes made to the model formulation.

The global Hg model is based on the three-dimensional (3D) CTM developed at the Goddard Institute for Space Studies (GISS), Harvard University, and the University of California at Irvine. The 3D model provides a horizontal resolution of 8° latitude and 10° longitude and a vertical resolution of nine layers ranging from the Earth's surface to the lower stratosphere. Seven layers are in the troposphere (between the surface and ~12 km altitude), and two layers are in the stratosphere (between ~12 and 30 km altitude).

Transport processes are driven by the wind fields and convection statistics calculated every 4 h (for 1 year) by the GISS general circulation model (*14*). This 1-year data set is used repeatedly for multiyear simulations until steady state is achieved.

The Hg transformation processes include gas-phase transformations, gas/droplet equilibria, ionic equilibria, solution/particle adsorption equilibrium, and aqueous-phase transformations as described above. The chemical species reacting with Hg are input to the model as described by Seigneur et al. (*1*).

The dry deposition velocity of Hg(II) was selected by analogy with that of nitric acid because of similar solubility. Measurements of nitric acid dry deposition velocities are in the range of 0.06−5 cm/s (*15*) with a mean value of 0.5 cm/s (*16*). We selected an average dry deposition velocity of 0.5 cm/s. The dry deposition velocity of Hg(0) has been estimated to be 0.09 cm/s under typical summer conditions over a forest canopy in Tennessee (*17*). Model simulations using a bi-directional atmosphere−surface exchange model led to a range of 0.02−0.15 cm/s, with an average value of 0.06 cm/s over plant canopies (*18*). However, experimental data suggest that the uptake of Hg(0) by vegetation occurs only when the atmospheric concentration of Hg(0) exceeds a threshold value referred to as the compensation point (*19*). For white oak, red maple, Norway spruce, and yellow poplar, the compensation points were estimated to be in the range of 10−25 ng/m^3, that is, above typical background annual average Hg(0) concentrations. Therefore, the deposition velocities reported above should be seen as upper limits because no Hg(0) deposition may occur when Hg(0) ambient concentrations are below the vegetation compensation points. Consequently, we selected the Hg(0) dry deposition velocity to be 0.01 cm/s over land and, because of its low solubility, 0 over the oceans. The Hg(p) deposition velocity was selected to be 0.1 cm/s over land and 0.01 cm/s over water; these values are typical for fine particles (e.g., assuming a particle diameter of 0.3 μm and a surface roughness of 0.1−1 m over land and 0.1−1 cm over water) (*20*). The value over land is consistent with the Hg(p) deposition velocity of 0.1 cm/s estimated for a typical summer day over a forest canopy in Tennessee (*17*).

Wet deposition is calculated using the cloud droplet chemical concentrations and the precipitation patterns. For below-cloud scavenging, we assumed no scavenging of Hg(0), 100% scavenging of Hg(II), and 50% scavenging of Hg(p). The Hg emissions consisted of Hg(0), Hg(II), and Hg(p) gridded emissions for anthropogenic and background sources as described below.

Continental Mercury Chemical Transport Model. The formulation of the continental CTM, TEAM, has been described in detail elsewhere (*1*, *21*). We present here an overview of the model and point out the major modifications made since its initial application.

TEAM is a 3D Eulerian model that simulates the transport, chemical and physical transformations, and wet and dry depositions of Hg species. In this application to North America, the horizontal grid resolution is 100 km, and the vertical grid consists of six layers from the surface to 6 km altitude with finer resolution near the surface (the layer interfaces are at 60, 150, 450, 850, and 2000 m). Transport processes include transport by the 3D mean wind flow and dispersion by atmospheric turbulence. The module that simulates the chemical and physical transformations of Hg described above is the same module as that used in the global model. Three Hg species, Hg(0), Hg(II), and Hg(p), are simulated. Hg(II) actually consists of several chemical species in the gas phase and in cloud droplets; Hg(II) can also adsorb to particulate matter (PM) in droplets.

Wet deposition is simulated only for Hg(II) and Hg(p) because Hg(0) is relatively insoluble. The wet deposition flux is calculated as the product of the cloud droplet concentration of the Hg species and the precipitation amount. Scavenging of these Hg species by rain below the cloud (washout) is treated as a transient process using scavenging coefficients that depend on precipitation intensity (*1*).

Dry deposition is simulated using the resistance transfer approach. The deposition process is simulated as a series of three mass transfer steps: (1) turbulent transport from the bulk atmosphere to near the surface, (2) diffusion through a laminar layer near the surface, and (3) uptake of the gas

TABLE 1. Anthropogenic Hg Emissions in the North American Domain (Mg/year)

source category	United States	southern Canada	northern Mexico	total	refs[a]
electric utilities	41.5	1.3	9.9	52.7	*22–25*
waste incineration	28.8	3.4	*b*	32.2	*25–28*
residential, commercial, and industrial coal burning	12.8	*b*	*b*	12.8	*25*
mining	6.4	0.3	*b*	6.7	*25, 29*
chlor-alkali facilities	6.7	0.05	*b*	6.8	*29, 30*
mobile sources	24.8	*b*	*b*	24.8	*31*
other sources	30.9	9.6	23.6	64.1	*1, 25*
total	**151.9**	**14.7**	**33.5**	**200.1**	

[a] See refs *1* and *25* for more detail on the development of the emission inventory. [b] Included in "other sources".

or particle by the surface. In the earlier formulation of TEAM, background emissions and dry deposition of Hg(0) were assumed to balance each other over North America. This assumption was justified by the fact that the atmospheric lifetime of Hg(0) (a few months) greatly exceeds its residence time (a few days) within the North American domain. In this current formulation, we explicitly treat the background emissions of Hg(0) and its dry deposition. The background emissions of Hg(0) include natural emissions from Mount St. Helen and from the mercuriferous areas of the western part of the domain (ranging from southern Canada to northern Mexico), as well as re-emissions of deposited mercury. We assumed that 50% of deposited mercury was re-emitted (see discussion of emissions below). For consistency with the global model, the dry deposition of Hg(0) was selected to be ~0.01 cm/s on average. For Hg(II), the dry deposition characteristics are assumed to be similar to those of nitric acid (HNO_3) because these two gases have similar solubilities. Dry deposition velocities calculated by TEAM for Hg(II) and Hg(p) over various surface types (forest, agricultural land, and water) are those used by Pai et al. (*21*) with the updates described by Seigneur et al. (*1*).

Emissions

North American Emissions. The North American anthropogenic mercury emission inventory is summarized by source category in Table 1. It is based on an earlier inventory (*1*). For the United States, some source categories (coal-fired power plants and chlor-alkali facilities) were updated and some source categories (mobile sources, landfills, and electric arc furnaces) were added. For coal-fired power plants, a new emission inventory provided by EPRI (*22*) was used. This inventory reflected the recent data on mercury coal content collected at all coal-fired power plants and stack measurements of speciated mercury conducted at >80 power plants as part of the U.S. Environmental Protection Agency (EPA) Information Collection Request (ICR) program. For chlor-alkali plants, a Wisconsin facility was added. That facility had been overlooked in the previous inventory because its emissions had not been reported in the 1998 Toxics Release Inventory (TRI) (*29*); nevertheless, this facility is still in operation. For mobile sources, the emission value (25 Mg/year) from the recent 1999 National Toxics Inventory (NTI) of the EPA (*31*) was used (an increase of 9 Mg/year from the earlier inventory). These mobile source emissions were obtained on a county-level basis and distributed uniformly over each county. Emissions from landfills (0.23 Mg/year) were distributed as area sources according to county data, and emissions from electric arc furnaces (0.014 Mg/year) were distributed according to their exact point source location. No changes were made to the Canadian and Mexican emission inventories.

Global Emissions. No changes were made to global anthropogenic mercury emissions besides those listed above for the United States. Anthropogenic emissions amount to 2143 Mg/year and consist of 246, 209, 176, 1138, 326, and 48 Mg/year for Africa, North America, Central and South America, Asia, Europe, and Oceania, respectively. One source category, volcanoes, was added to the inventory of natural emissions of Seigneur et al. (*1*). Natural emissions consist now of three source categories: mercury-enriched land areas, volcanoes, and oceans.

Direct emissions from mercury-enriched land areas amount to 500 Mg/year in our base inventory. They are uniformly distributed according to a global map of natural enrichment of mercury as reported in Figure 1 of Gustin et al. (*32*). As a check on this estimate, this value corresponds to ~10 Mg/year for Nevada when scaled by land area. This value is consistent with the estimate of 9.4 Mg/year derived by Zehner and Gustin (*33*) from experimental data (they assumed that 30% of mercury deposited—with a wet/dry deposition ratio of 1—was re-emitted).

Volcanic emissions were estimated to be 125 Mg/year for 1998. First, the activity of volcanoes was characterized (i.e., erupting and/or degassing) (*34*). Next, the emissions associated with eruption were estimated by obtaining volcano-specific information on the number of days of eruption during 1998 (*35*). Emission factors for eruption and degassing were obtained from Nriagu and Becker (*36*). This source category was then spatially distributed according to the location of those active volcanoes.

Emissions from oceans include direct emissions and re-emissions of natural and anthropogenic mercury. In our base inventory, emissions from oceans amount to ~2000 Mg/year. Mason and Sheu (*37*) recently estimated total emissions of mercury from oceans at 2600 Mg/year. However, they considered that a significant fraction of the Hg(0) emitted was rapidly oxidized to Hg(II) in the marine boundary layer and deposited back to the ocean. They estimated the total net flux out of the marine boundary layer to be 1460 Mg/year. Our global model accounts for some oxidation process that can occur within the marine boundary layer (aqueous oxidation by Cl_2); however, the coarse spatial resolution required by the global scale simulation does not allow for a sufficiently detailed representation of the processes occurring within the marine boundary layer. Therefore, it seems to be appropriate that our estimate of emissions from oceans lies within the range of the gross and net fluxes estimated by Mason and Sheu (*37*).

Emissions of mercury also occur during vegetation fires. Friedli et al. (*38, 39*) have reported laboratory and field experimental data. When those data are extrapolated to a global biomass inventory, estimates of mercury emissions from biomass burning range from ~100 to 800 Mg/year (*38*). Such emissions are likely to correspond to the re-emission of mercury previously deposited to the vegetation or the underlying soil. Therefore, we did not include a separate category for mercury emissions from fires in our global emission inventory because such emissions are assumed to be included in the re-emissions.

Re-emissions constitute the difference between the total emissions and the direct (both anthropogenic and natural) emissions (see below).

Emission Scenarios. The global mercury emission budget, T (Mg/y), can be expressed as

$$T = A_d + A_r + N_d + N_r \quad (1)$$

where A_d represents the direct anthropogenic emissions, A_r represents the re-emissions of anthropogenic mercury, N_d

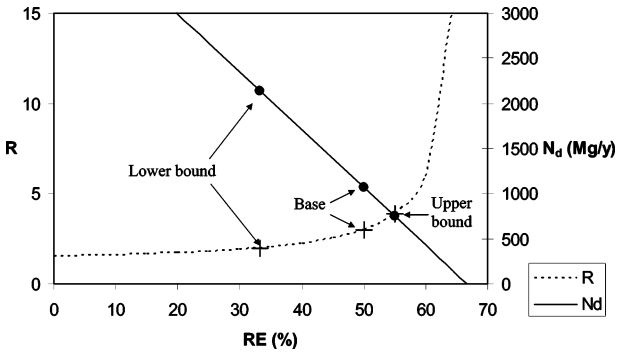

FIGURE 1. Natural direct emissions (N_d) and ratio of current/pre-industrial emissions (R) as functions of the re-emissions of deposited mercury (RE).

represents the direct natural emissions, and N_r represents the re-emissions of natural mercury. The ratio of current emissions to pre-industrial (i.e., natural) emissions, R, is then defined as follows:

$$R = T/(N_d + N_r) \quad (2)$$

The percentage of deposited mercury that is re-emitted, RE, is defined as follows:

$$\mathrm{RE} = 100 \times (A_r + N_r)/T \quad (3)$$

In our base scenario, we assume that current emissions are 3 times greater than pre-industrial emissions, that is, $R = 3$. Therefore, natural emissions are half of the anthropogenic emissions, that is, 1067 Mg/year (derived from an anthropogenic value of 2134 Mg/year prior to the update of the U.S. mobile sources, see Supporting Information), and total direct emissions are 3210 Mg/year. We also assume that half of deposited mercury (both natural and anthropogenic) is being re-emitted, that is, RE = 50%. Because the amount of mercury emitted must equal the amount deposited, re-emissions account for half of the total emissions.

There are some significant uncertainties in the estimates of background emissions, for example, the magnitude of natural emissions as well as the fraction of deposited mercury that is re-emitted. To address those uncertainties, we considered two alternative scenarios. We constrained the total global emissions and the direct anthropogenic emissions to the values listed above, that is, 6411 and 2143 Mg/year, respectively. Thus, background emissions amount to 4268 Mg/year to be distributed among direct natural emissions, re-emissions of natural mercury, and re-emissions of anthropogenic mercury. Figure 1 presents the direct natural emissions as a function of RE. Also shown in Figure 1 is the ratio of current emissions to pre-industrial emissions, R, as a function of RE. (See Supporting Information for more detail on the global emissions and the functions presented in Figure 1.)

Measurements of mercury concentrations in sediments and peat cores suggest that current mercury global concentrations are 1.5−12 times those of pre-industrial times (*40*−*45*). The most recent analyses are discussed below. The analysis of peat bog and lake sediments in Nova Scotia and New Zealand by Lamborg et al. (*42*) led those authors to estimate a ratio of current/pre-industrial deposition fluxes of ~4. Schuster et al. (*43*) analyzed ice-core samples in the Upper Fremont Glacier in Wyoming and estimated a ratio of 11. Bindler (*44*) sampled peat cores in south-central Sweden and estimated a ratio of at least 10. Roos-Barraclough and Shotyk (*45*) sampled peat cores at two nearby sites in Switzerland and estimated a ratio of 11−12.

When using such data to estimate the ratio of current and pre-industrial emissions, one assumes that the ratio of deposition fluxes can be applied to emissions. This is an approximation because anthropogenic emissions include gaseous Hg(II) and Hg(p), which are deposited closer to their source than Hg(0) and, therefore, may not enter the global background, and atmospheric concentrations of reactants such as O_3, SO_2, OH, and HO_2 have changed from pre-industrial times to current times.

Figure 1 shows that a value of $R > 6$ requires that >60% of deposited mercury be re-emitted. Also, a value of $R > 6$ leads to natural emissions of <400 Mg/year, which seems inconsistent with estimates of natural emissions from volcanoes (~100 Mg/year) and mercuriferous belts (~500 Mg/year). Therefore, estimates of a ratio of current/pre-industrial deposition fluxes of >6 may reflect a local or regional mercury deposition pattern and may not be representative of a globally averaged ratio of current emissions to pre-industrial emissions.

There is no comprehensive information on mercury re-emissions because this process is likely to depend on surface type and meteorological conditions. Gustin (*46*) assumed that 30% of deposited mercury was re-emitted in her analysis of natural mercury emissions in Nevada. Recent data from the Experimental Lakes Area in Canada suggest that 8% of applied mercury was re-emitted the first year and that 16% of "native" mercury was re-emitted (*47*). Landis and Keeler (*48*) estimated mercury deposition to and evasion from Lake Michigan using data from the Lake Michigan Mass Balance Study. They estimated that, on an annual basis, evasion of Hg(0) from the lake amounted to 38% of wet and dry deposition of mercury to the lake. A lower percentage of re-emitted mercury leads to a larger fraction of direct natural mercury emissions if the direct anthropogenic and total global emissions are fixed (see Figure 1).

For this study, we selected three scenarios. In our base scenario, we assumed that 50% of deposited mercury is re-emitted to the atmosphere; this corresponds to a ratio of current/pre-industrial emissions, R, of 3, that is, similar to that of Mason and Sheu (*37*). In one alternative scenario (hereafter referred to as the lower bound scenario), we assumed that 33% of deposited mercury is re-emitted; this corresponds to $R = 2$. This ratio of current/pre-industrial emissions is toward the low part of the range reported in the literature. On the other hand, the re-emitted fraction may be more consistent with the preliminary estimates discussed above. In the other alternative scenario (hereafter referred to as the upper bound scenario), we assumed that 56% of deposited mercury is re-emitted; this corresponds to $R = 4$, that is, a ratio of current/pre-industrial emissions identical to that of Lamborg et al. (*42*).

The emissions from land and oceans vary little among those scenarios because the mercury background emissions are redistributed among their direct natural emissions, re-emissions of natural mercury, and re-emissions of anthropogenic mercury. Emissions from land range from 2266 Mg/year (upper bound scenario) to 2360 Mg/year (lower bound scenario), whereas emissions from oceans range from 1908 Mg/year (lower bound scenario) to 2002 Mg/year (upper bound scenario).

Figure 2 presents a summary of the global mercury budget for our base emission scenario. Because it is not possible to differentiate between natural and anthropogenic mercury after it has been emitted, re-emissions must necessarily include both natural and anthropogenic mercury. These re-emissions are allocated to both natural and anthropogenic emissions, proportionately to the direct emissions.

TABLE 2. Comparison of Recent Global Budgets for Atmospheric Mercury

emissions	Bergan et al. (*49*)	Mason and Sheu (*37*)	Lamborg et al. (*42*)	this work, base	this work, lower bound	this work, upper bound
direct anthropogenic (Mg/year)	2160	2400		2143	2143	2143
re-emitted anthropogenic (Mg/year)	2000	2090	4800	2134	1067	2670
natural from land[a] (Mg/year)	500	810	1000	1180	1805	878
natural from oceans[a] (Mg/year)	1400	1300	600	954	1396	720
total (Mg/year)	6060	6600	6400	6411	6411	6411
re-emissions/deposition (%)	50	47	NA[b]	50	33	56
current/pre-industrial emissions	3	3.1	4	3	2	4

[a] Including re-emission of natural mercury. [b] Not available.

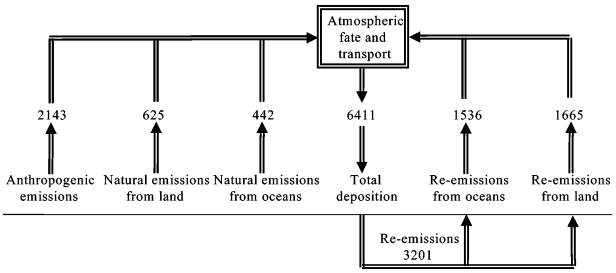

FIGURE 2. Schematic summary of the global atmospheric mercury cycle for the base emission scenario (annual emission and deposition rates are in Mg/year).

Table 2 compares some recent global mercury budgets. Direct anthropogenic emissions range from 2143 to 2400 Mg/year. Natural land emissions (including re-emissions of natural mercury) range from 500 Mg/year (*49*) to 1805 Mg/year (lower bound scenario). Natural emissions from oceans (including re-emissions of natural mercury) range from 600 Mg/year (*42*) to 1396 Mg/year (lower bound scenario). Re-emissions of anthropogenic mercury range from 1067 Mg/year (lower bound scenario) to 2670 Mg/year (upper bound scenario). The ratio of current emissions to pre-industrial emissions of our base scenario is consistent with those used by Bergan et al. (*49*) and Mason and Sheu (*37*). The percentage of deposited mercury that is re-emitted in our base scenario is also consistent with those used by Bergan et al. (*49*) and by Mason and Sheu (*37*).

Performance Evaluation of the Global and Continental Models

Prior to the conducting of a source attribution analysis with this global/continental modeling system, it is essential to evaluate the performance of the two CTMs to ensure that they can reproduce the major characteristics observed in measurements of mercury concentrations and deposition fluxes as well as to assess their current limitations. To that end, we present below the evaluation of the global and continental model simulation results against available data.

Global Mercury Chemical Transport Model. Figure 3 presents the global ground-level annual-average concentrations of Hg(0), Hg(II), and Hg(p). The surface Hg(0) concentrations display a strong latitudinal gradient with background concentrations mostly in the range of 1.2−1.6 ng/m^3 in the southern hemisphere and mostly in the range of 1.6−1.9 ng/m^3 in the northern hemisphere. Concentrations >1.7 ng/m^3 are simulated over the large source areas of eastern Europe and eastern Asia. In the southern hemisphere, South Africa shows up as a large source area with Hg(0) concentrations up to 1.6 ng/m^3.

The Hg(II) concentrations show stronger spatial variations than the Hg(0) concentrations due to their stronger correlations with source areas, such as South Africa, North America, Europe, and Asia. The highest Hg(II) concentrations (>100 pg/m^3) are simulated over eastern China, due to the fact that Asia accounts for half of the global anthropogenic emissions.

The Hg(p) concentrations are solely of anthropogenic origin and, therefore, they provide footprints of the major source areas. Concentrations of Hg(p) in eastern Asia are in the range of 100−200 pg/m^3.

The average atmospheric lifetime of mercury was calculated to be 1.2 years. Table 3 presents a comparison of simulated mercury concentrations with mercury concentrations measured at a variety of locations. Those concentrations measured in North America are compared below with the results of the continental simulation. In Europe, the simulated concentrations of total gaseous mercury (TGM) [represented by the sum of Hg(0) and Hg(II) in the model] are within 6% (0.12 ng/m^3) of the measurements at the Mace Head site on the west coast of Ireland and at various sites in Germany, but are underpredicted by about 30% (0.8 ng/m^3) in Slovakia and by 12% (0.25 ng/m^3) in Tuscany, Italy, and overpredicted by about 9−17% (0.14−0.25 ng/m^3) in Sweden. The underpredictions are likely due to the coarse spatial resolution of the global model, which tends to dilute primary emissions of mercury. The overprediction in Scandinavia may be due to an underestimation of dry deposition over forested areas in the global model. In Asia, the model underpredicts TGM concentrations by 40−50% (1−2 ng/m^3) in Korea and underpredicts by several nanograms per cubic meter in southern Kyushu, Japan, and in Beijing, China. These large underpredictions result from the fact that those latter measurements do not reflect background concentrations but rather correspond to the local impacts of nearby sources. For example, in Beijing, most homes burn coal for heating and cooking, thereby causing large emissions of mercury within a small area. Measurements in such an area will then reflect primarily local emissions. In southern Kyushu, Japan, the measurements were taken near an active volcano. This volcano is an important local source of mercury that is diluted within the global model coarse resolution. The simulated TGM concentration of 1.48 ng/m^3 in the Amazon is consistent with the range reported here for clean conditions. The model underpredicts the TGM concentration in South Africa by 0.25 ng/m^3. The TGM concentrations measured in the southern Atlantic Ocean are correctly predicted. However, the TGM concentrations measured in the northern Atlantic Ocean tend to be underpredicted by 20%. Thus, the model correctly predicts the direction of the north/south gradient in TGM concentrations but tends to underestimate the slope of that gradient. The Hg(0) concentrations measured in marine air at Cheeka Peak Observatory, WA, are representative of concentrations over the Pacific Ocean. The model correctly predicts the range of observed Hg(0) concentrations and reproduces the summer/winter seasonality. However, both RGM and TPM in the marine boundary layer are overpredicted by the model.

The simulated TPM concentration in Changchun, China, is at the lower range of the measurements because the coarse

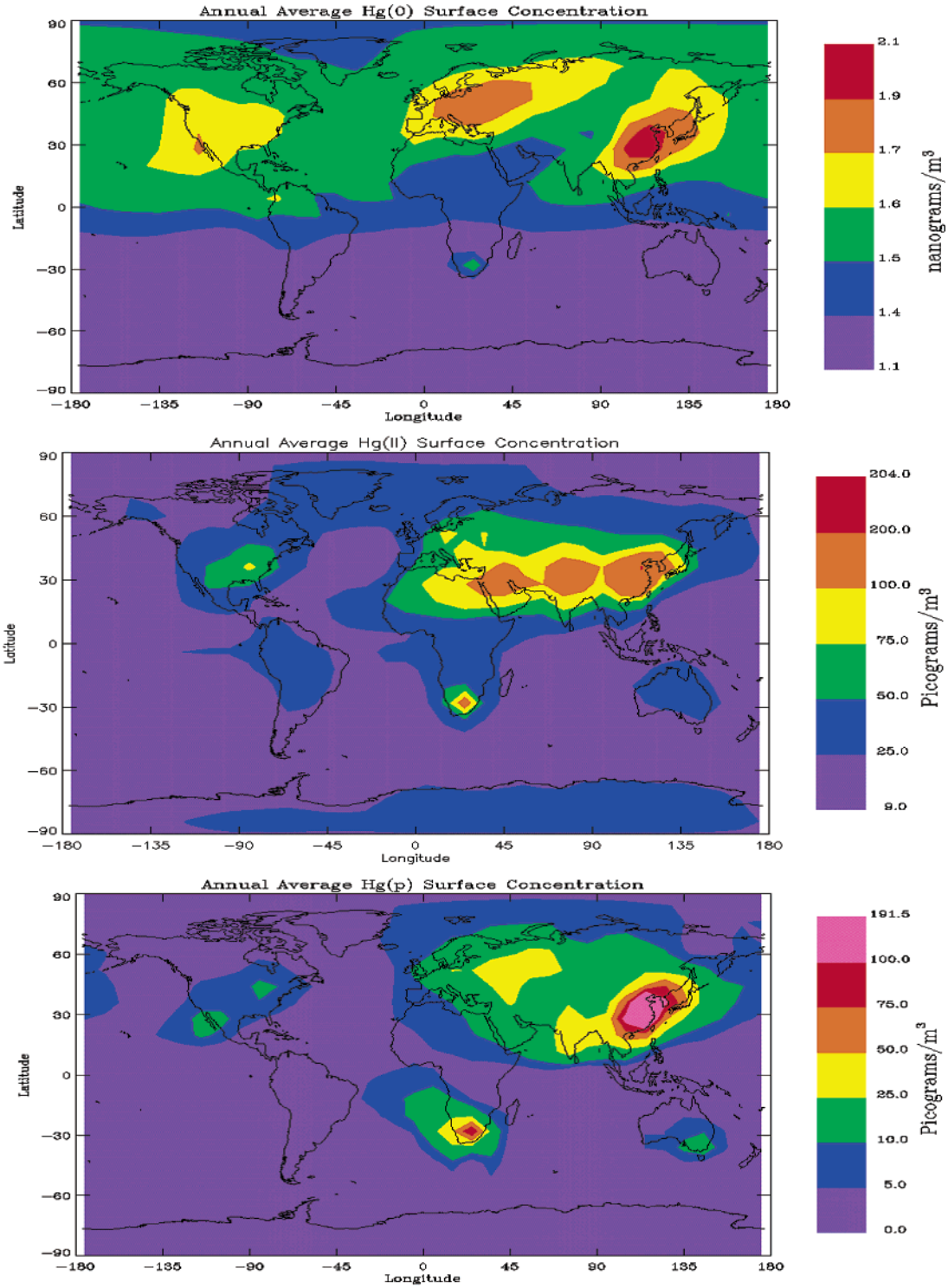

FIGURE 3. Global annual-average surface concentrations of Hg(0) (ng/m^3, top), Hg(II) (pg/m^3, middle), and Hg(p) (pg/m^3, bottom).

grid size dilutes the impact of local sources. The measurements conducted in Tuscany included speciated mercury concentrations. The model appears to overpredict the reactive gaseous mercury (RGM) concentration [represented by Hg(II) in the model] and to underpredict the total particulate mercury (TPM) concentration [represented by Hg(p) in the model]. This suggests that some RGM may adsorb to atmospheric particulate matter (PM), a process that is simulated in the cloud droplets but is assumed to be reversible (i.e., in the model, RGM returns to the gas phase after evaporation of the cloud droplets).

Continental Mercury Chemical Transport Model. Figure 4 depicts the annual-average concentrations of Hg(0), Hg(II), and Hg(p) over the contiguous United States. Maximum Hg(0) concentrations reach 4.4 ng/m^3. Overall, Hg(0) concentrations are high (>2 ng/m^3) in the western United States because of natural emissions and re-emissions of mercury deposited mainly via precipitation, low in the central United States (<1.7 ng/m^3), and moderately high (>1.7 ng/m^3) in the eastern United States because of anthropogenic emissions. For the most part, Hg(II) concentrations are higher in the eastern United States than in the western United States,

TABLE 3. Comparison of Observed and Simulated Mercury Concentrations (ng/m^3)

location	period	species	observation[a]	simulation	refs
		United States			
Cheeka Peak Observatory, WA; marine air	May 2001−May 2002; spring; summer; fall; winter	Hg(0)	1.54; 1.61; 1.54; 1.51	1.60; 1.60; 1.55; 1.55	*50*
		RGM	0.0016; NA; <0.0016; <0.0016	0.013; 0.012; 0.0096; 0.032	
		TPM	0.0005; <0.0004; NA; NA	0.004; 0.002; 0.003; 0.0055	
Cheeka Peak Observatory, WA; continental air	May 2001−May 2002; spring; summer; fall; winter	Hg(0)	1.46; 1.50; 1.49; 1.47	2.15; 2.17; 2.02; 2.00	*50*
		RGM	0.0027; NA; 0.002; <0.0016	0.011; 0.017; 0.007; 0.007	
		TPM	0.0015; 0.0029; NA; NA	0.002; 0.0034; 0.0019; 0.0022	
Steamboat Springs, NV	Sept 1997	TGM	2−200	2.27	*32*
Cheasapeake Bay, MD	1997−1999	Hg(0)	1.89	1.85	*51*
		RGM	0.04	0.06	
		TPM	0.02	0.01	
Eagle Harbor, MI	Aug 1997	TGM	1.2	1.6	*52*
		TPM	0.008	0.003	
Dexter, MI	Oct 1997; Sept 1998	TGM	1.5; 1.5	2.3; 2.3	*52*
		TPM	0.014; 0.013	0.003; 0.003	
Everglades, FL	March 1999	TGM	1.9	1.7	*52*
		TPM	0.025	0.005	
Caryville, FL	1995−1996	TPM	0.006	0.003	*53*
Lake Barco, FL	1994−1996	TPM	0.006	0.003	*53*
southern Florida	1994−1996	TPM	0.002−0.009	0.006	*53*
Barrow, AK	Feb 1999−April 2001	RGM	0.024	0.021	*54*
Baltimore, MD	Feb 1999−April 2001	RGM	0.023	0.183	*54*
Durham, NC	Feb 1999−April 2001	RGM	0.016	0.034	*54*
Everglades, FL	Feb 1999−April 2001	RGM	0.015	0.060	*54*
Pompano Beach, FL	June 2000	TGM	2.0	2.1	*55*
		RGM	0.005	0.020	
		TPM ($PM_{2.5}$)	0.002	0.005	
		TPM (PM_{10})	0.015		
		Canada			
Alert, NT	1997−1999	TGM	1.55	1.52	*56*
Esther, AB	1997−1999	TGM	1.69	1.39	*56*
Mingan, PQ	1997−1999	TGM	1.62	1.57	*56, 57*
Reifel Island, BC	1997−1999	TGM	1.69	2.60	*56*
Burnt Island, ON	1997−1999	TGM	1.58	1.66	*56*
St. Anicet, PQ	1997−1999	TGM	1.72	1.91	*56, 57*
St. Andrews, NB	1997−1999	TGM	1.43	1.45	*56*
Kejimkujik, NS	1997−1999	TGM	1.33	1.6	*56*
Egbert, ON	1997−1999	TGM	1.65	2.15	*56*
Point Petre, ON	1997−1999	TGM	1.9	1.74	*56*
L'Assomption, PQ	1998	TGM	1.79	2.48	*57*
Villeroy, PQ	1998	TGM	1.62	1.65	*57*
		Europe			
Mace Head, Ireland	1995−2001	TGM	1.75	1.64	*58*
Wank Mountain, Germany	1996	TGM	1.82	1.81	*59*
Slovak Republic	1996−1997	TGM	2.63	1.86	*60*
Tuscany, Italy	June 1998	TGM	2.0	1.75	*61*
		RGM	0.022	0.087	
		TPM	0.056	0.021	
Neuglobsow, Germany	1998−1999	TGM	1.98	1.86	*62*
Zingst, Germany	1998−1999	TGM	1.82	1.86	*62*
Roervik, Sweden	1998−1999	TGM	1.54	1.68	*62*
Aspvreten, Sweden	1998−1999	TGM	1.43	1.68	*62*
northwestern Europe and Mediterranean	1998−1999	RGM	0.010−0.065	0.017−0.083	*62*
		TPM	0.012−0.040	0.004−0.027	
		Asia			
western Korea	March 2001	TGM	3.72	2.13	*63*
Seoul, Korea	Sept 1997; May−June 1998	TGM	3.43−3.94	2.03; 2.12	*64*
Kyushu, Japan	1996	TGM	10.8	1.70	*65*
Beijing, China	Jan, Feb, Sept 1998	TGM	6.2−24.7	2.26; 2.38	*66*
Changchun, China	July 1999−Jan 2000	TPM	0.02−2	0.062	*67*
		South America			
Amazon	Aug−Sept 1995	TGM	0.5−2	1.48	*68*
		Africa			
Cape Point, South Africa	Dec 1999−Jan 2000	TGM	1.29	1.04	*69*
		Atlantic Ocean			
Northern Hemisphere	Dec 1999−Jan 2000	TGM	2.0	1.6	*70*
Southern Hemisphere	Dec 1999−Jan 2000	TGM	1.3	1.3	*70*

[a] Mean value of measurements.

although a few isolated grid cells in the west show concentrations >50 pg/m^3. Hg(II) concentrations are mostly <100 pg/m^3, except for a few grid cells that show concentrations in the range of 100−183 pg/m^3. In northern California, the high Hg(II) concentration corresponds to the Geysers area, where we assumed 30% Hg(II) for the emissions; high Hg(II)

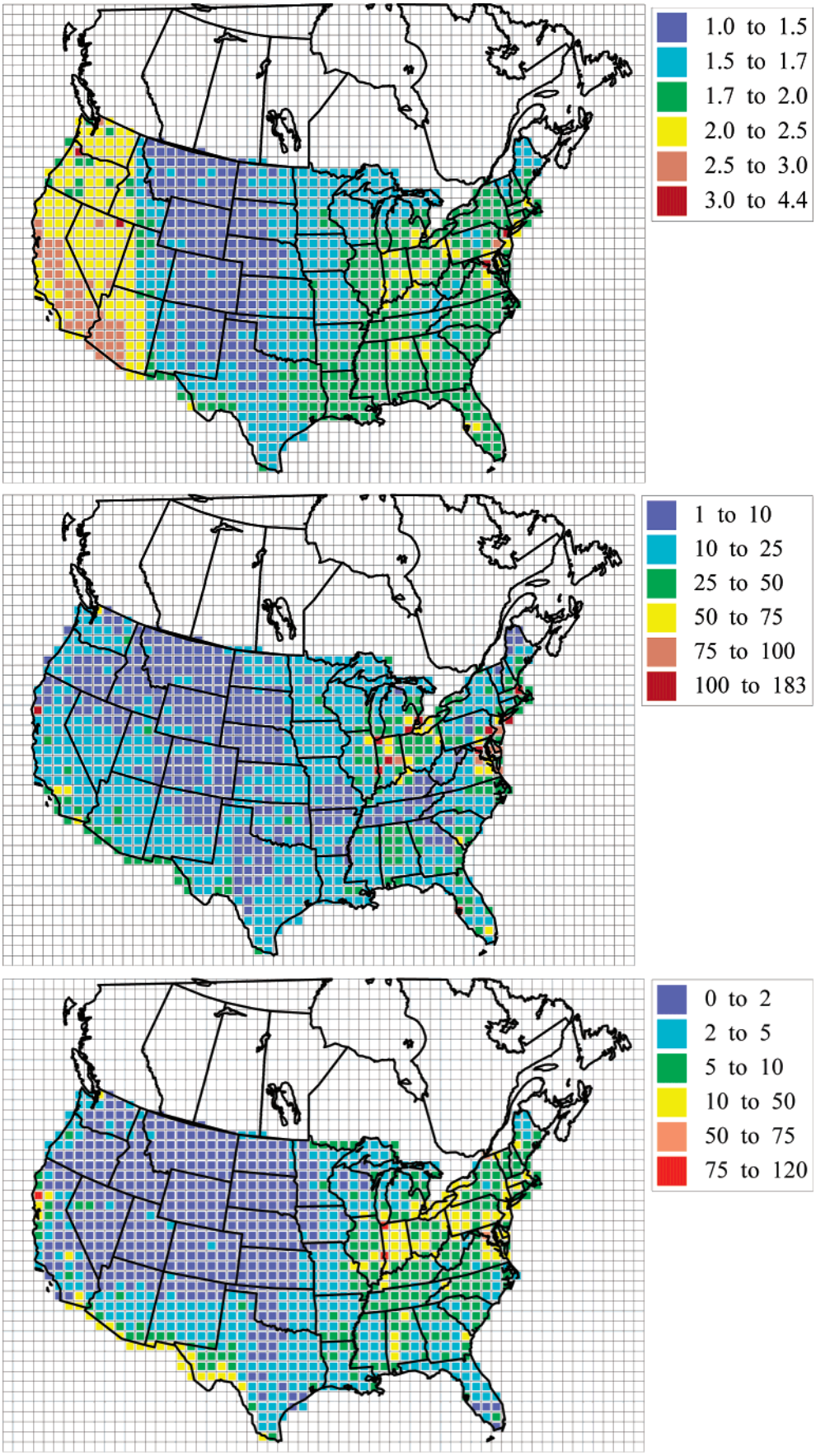

FIGURE 4. U.S. annual-average surface concentrations of Hg(0) (ng/m^3, top), Hg(II) (pg/m^3, middle), and Hg(p) (pg/m^3, bottom).

concentrations have been measured in an area with some geothermal activity, Sulfur Banks, CA (*46*). Hg(p) concentrations reach 120 pg/m^3 in some grid cells but are primarily <50 pg/m^3.

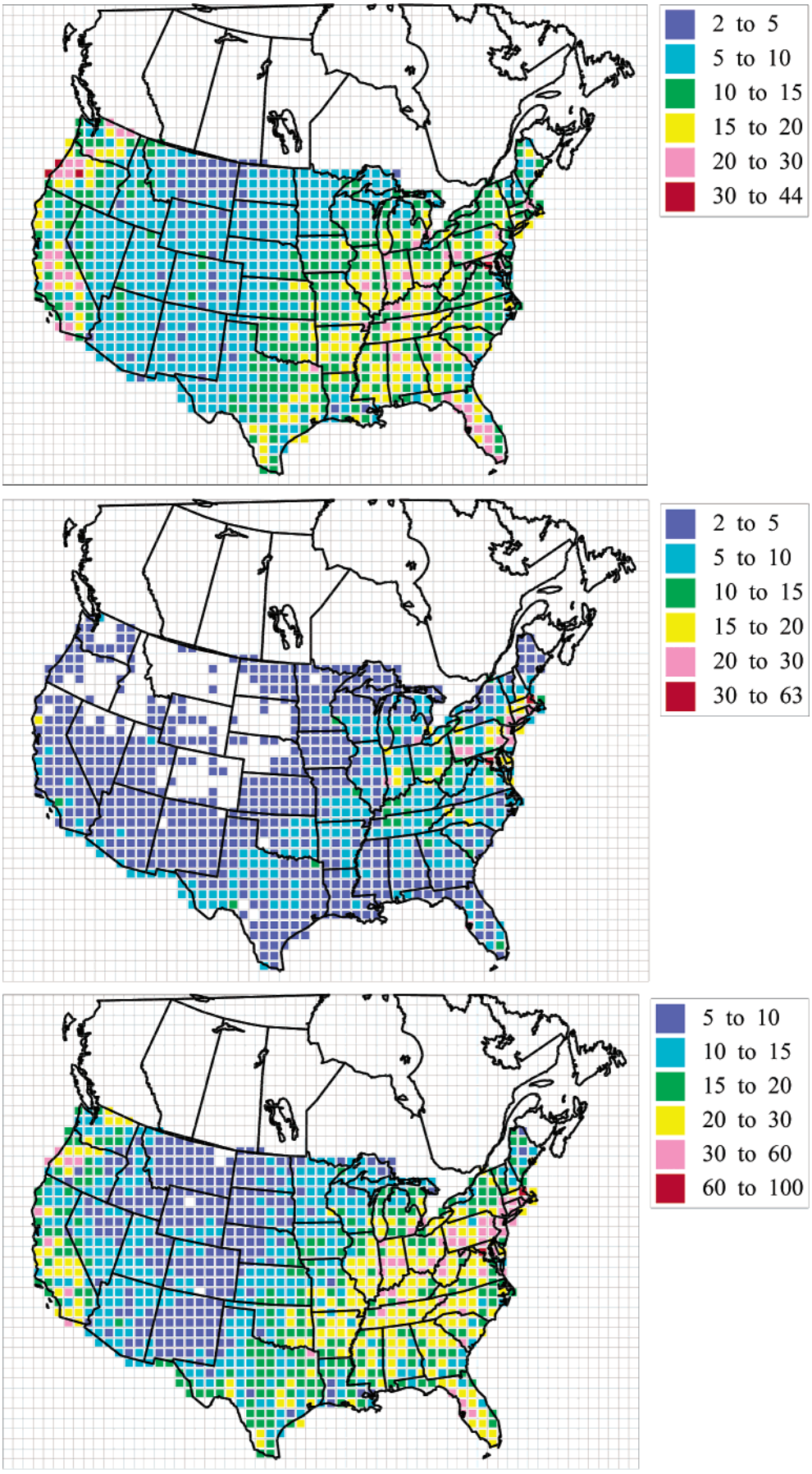

FIGURE 5. U.S. annual wet deposition flux (μg/m^2-year, top), dry deposition flux (μg/m^2-year, middle), and total deposition flux of total Hg (μg/m^2-year, bottom).

Figure 5 depicts the wet, dry, and total (i.e., wet plus dry) mercury deposition fluxes over the contiguous United States. Wet deposition fluxes are highest in the western and eastern United States. The high wet deposition fluxes on the west coast are due to the global Hg(II) concentrations at the upwind boundary (25 pg/m^3 on average) as well as high precipitation along the mountain ranges of the Cascades and Sierra Nevada. The high wet deposition fluxes in the eastern United States result from the influence of local/regional sources (e.g., in the northeast) or high precipitation (e.g., Florida). Dry deposition fluxes are highest in the northeastern United States. The high (15−20 μg/m^2-year) dry deposition flux in northern California corresponds to the Geysers area. The high dry deposition fluxes in the northeast result from the impacts of local/regional emission sources. The total deposition fluxes reflect the characteristics mentioned above for the wet and dry deposition fluxes.

A comparison of observed and simulated concentrations of mercury is presented in Table 3 for several locations in the United States and Canada. In the United States, TGM concentrations are correctly predicted in the east (in Florida and Maryland) but are overpredicted in the midwest and northwest. In Nevada, the model prediction is consistent with the lower range of the measured concentrations; the high measured concentrations reflect the fact that the data were collected over mercury-enriched areas that are not resolved spatially by the model. In Canada, the model shows good agreement (i.e., within 0.1 ng/m^3) for TGM at five sites (Alert, Mingan, Burnt Island, St. Andrews, and Villeroy), underpredicts at two sites by up to 0.3 ng/m^3 (Esther and Point Petre), and overpredicts at the other five sites by 0.2−0.9 ng/m^3. The large simulated concentration of 2.6 ng/m^3 at Reifel Island is due to the presence of several large sources (a chlor-alkali plant and incinerators) in the Seattle area. The large simulated concentration of 2.48 ng/m^3 at L'Assomption is due to the fact that Montreal is located in the same grid cell.

The model correctly predicts the RGM concentration at Barrow, AK, but overpredicts RGM concentrations within the contiguous United States. The significant overprediction in Baltimore is in part due to the local impact of a municipal waste incinerator in the 1998 model simulation; the implementation of emission controls in the 1999−2000 period is likely reflected in the measurements. The overall overprediction of RGM may be due to the fact that some Hg(II) is actually adsorbed to atmospheric PM [see discussion of Tuscany measurements above and discussion of Mace Head measurements by Seigneur et al. (*1*)] and is not measured as RGM but may be present as TPM. This is consistent with the fact that the model tends to underpredict TPM at most sites. In Maryland, where both RGM and TPM were measured concurrently, the model agrees well with the measurements of the sum of RGM and TPM. However, in Washington state, the model overestimates both RGM and TPM, although it correctly predicts greater RGM than TPM concentrations in continental air and in marine air.

Mason et al. (*71*) reported fluxes of mercury wet deposition at four sites (one urban and three rural) in Maryland. A direct comparison with the simulated values is not feasible because the observed annual deposition fluxes are reported for May 1997−May 1998, whereas the model simulation is for the year 1998, and there is considerable year-to-year variability. It is, nevertheless, interesting to compare differences between the urban site and the rural sites. Mason et al. report that wet deposition at the urban site is 2−3 times greater than at the rural sites. The model simulation shows a similar trend with wet deposition at the urban site being 1.7−4.4 times greater than at the rural sites.

For North America, we also compared modeled wet deposition fluxes of mercury to observations available for 1998 from the Mercury Deposition Network (MDN). Figure 6 presents the comparison for all 30 individual MDN sites. Some aspects of model performance improved from the previous version of the model (*72*). The coefficient of determination (r^2) increased from 0.45 to 0.50, the normalized error decreased from 28 to 25%, but the magnitude of the normalized bias increased slightly from −9 to +11%.

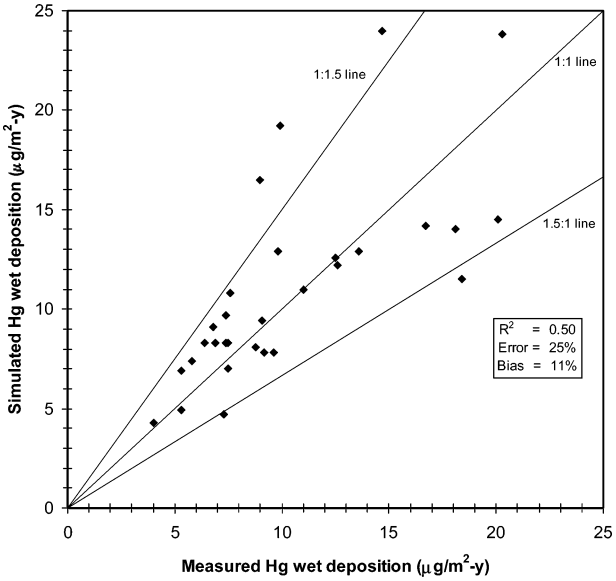

FIGURE 6. Comparison of simulated and observed mercury wet deposition fluxes for 1998 at individual MDN sites.

Global Source Attribution

Emission Sensitivity Simulations. Mercury is a global pollutant, and a significant fraction of the mercury deposition occurring within the United States is due to anthropogenic emissions from other continents, natural emissions, and re-emissions of mercury. It is, therefore, of interest to simulate the relative contributions of these global sources to mercury deposition in the United States. To that end, we conducted several simulations to estimate the following: (1) the effect of direct anthropogenic emissions (i.e., without their re-emissions) from individual continents; (2) the effect of direct natural emissions (i.e., without their re-emissions) from land and the oceans; (3) the effect of both direct and indirect (i.e., including re-emissions) anthropogenic emissions from individual continents, and (4) the effect of both direct and indirect (i.e., including re-emissions) natural emissions from land and the oceans.

To simulate the effect of direct anthropogenic or natural emissions, a global model simulation was conducted with only the source category of interest (i.e., anthropogenic emissions from a continent or natural emissions). The results of that simulation were then used to provide the boundary concentrations of the North American TEAM simulation reflecting the contribution of that source, and a TEAM simulation was then conducted to simulate the effect of that source. This approach is appropriate because the atmospheric transport and transformation processes of mercury are linear with respect to mercury species, and the results of simulations for individual sources are consequently additive.

The effect of the indirect component (i.e., re-emissions) of anthropogenic and natural sources was simulated as follows. A global simulation was conducted to obtain the contribution of re-emissions to the TEAM boundary conditions, and a TEAM simulation was conducted to calculate the corresponding contribution to mercury deposition in the United States. These re-emissions were then allocated

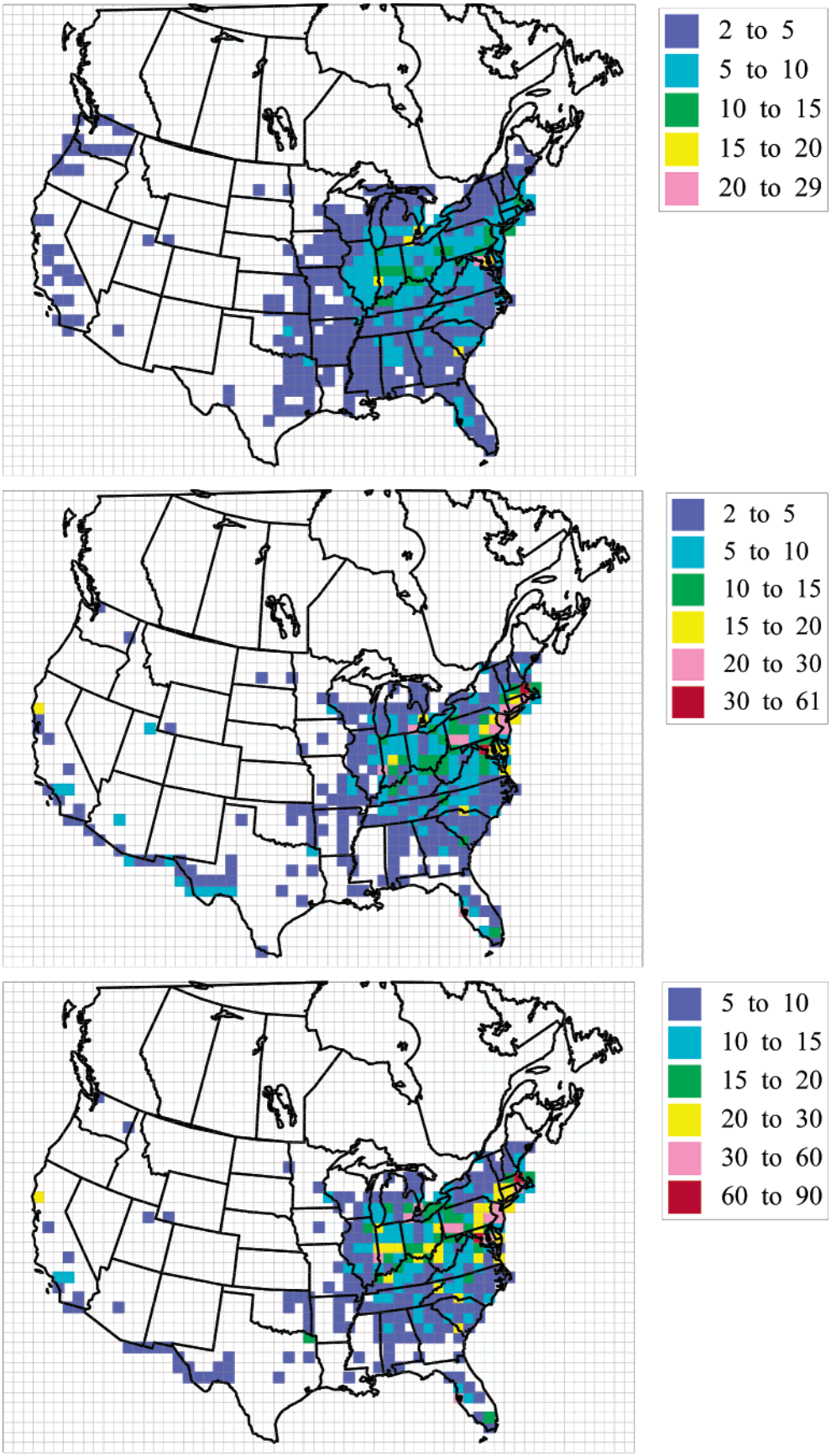

FIGURE 7. Annual wet (top), dry (middle), and total (bottom) deposition fluxes of total Hg (μg/m^2-year): contribution of North American anthropogenic emissions.

proportionately to the anthropogenic and natural sources according to their respective emission levels (e.g., in the base case, two-thirds of re-emissions were allocated to anthropogenic emissions and one-third to natural emissions; Asia

was allocated 53% of the anthropogenic fraction, North America, 10%, and so on).

In the results presented below, we consider deposition of only Hg(II) and Hg(p) following the methodology of Seigneur et al. (*3*).

Simulation Results. The contribution of North American direct anthropogenic emissions only (i.e., without the corresponding re-emissions) to mercury deposition occurring in the United States is presented in Figure 7 for wet, dry, and total deposition, respectively. It corresponds to a TEAM simulation conducted with North American emissions and boundary conditions corresponding to these emissions. The contribution to wet deposition west of the Mississippi river is <5 $\mu g/m^2$-year except for two grid cells that have wet deposition fluxes between 5 and 10 $\mu g/m^2$-year. In the eastern United States, the contribution is mostly in the range of 2−10 $\mu g/m^2$-year but reaches 29 $\mu g/m^2$-year in the mid-Atlantic region. The same patterns appear for dry deposition, but the contribution is greater in the eastern United States (up to 61 $\mu g/m^2$-year) because Hg(II) emissions can deposit locally and regionally via dry processes, whereas some fraction gets reduced to Hg(0) in the presence of clouds, which is not removed via wet deposition. Contributions of anthropogenic North American sources to total deposition of mercury are primarily limited to the eastern United States, with the largest contributions in the northeastern United States.

The contributions of direct anthropogenic emissions from other continents, direct natural emissions, and re-emissions to mercury deposition in the United States were simulated similarly, that is, by conducting a TEAM simulation with boundary conditions corresponding to the source of interest and with no North American emissions. Re-emissions were attributed to anthropogenic and natural emissions as described above. The contributions of anthropogenic and natural emissions, including their corresponding re-emissions, to wet, dry, and total mercury deposition in the contiguous United States are presented for the base emission scenario in Figure 8.

On average, North American anthropogenic emissions are calculated to contribute 30% to mercury total deposition in the contiguous United States; other anthropogenic emissions contribute 37%, with Asia contributing the most (21%), whereas natural emissions account for 33%. The results differ for the other two emission scenarios. For the lower bound scenario, which includes equivalent amounts of global natural and anthropogenic emissions, natural emissions dominate with 51% of mercury total deposition in the contiguous United States. North American anthropogenic emissions are calculated to contribute only 25%; other anthropogenic emissions contribute 24%, with Asia contributing the most (14%). For the upper bound scenario, which includes 3 times more anthropogenic emissions than natural emissions, North American anthropogenic emissions are calculated to contribute 32% of mercury total deposition in the contiguous United States. Other anthropogenic emissions contribute 42%, with Asia contributing 25%. Natural emissions account for only 26%. These results provide some estimate of the uncertainties associated with the relative distribution of background emissions between direct natural emissions and re-emissions of deposited mercury.

The contributions of anthropogenic and natural emissions to mercury deposition at specific receptors distributed across the continental United States were also analyzed. Nineteen receptors that represent a selection of areas that are potentially sensitive to mercury deposition were chosen for this analysis. Their locations are depicted in Figure 9. Those receptors are (in the order of their identification number in Figure 9): Brule River, WI (MDN site WI08); Devil's Lake, WI (MDN site WI31); Sleeping Bear Dunes National Lakeshore, MI; Lake Erie, PA (MDN site PA30); Huntington Wildlife

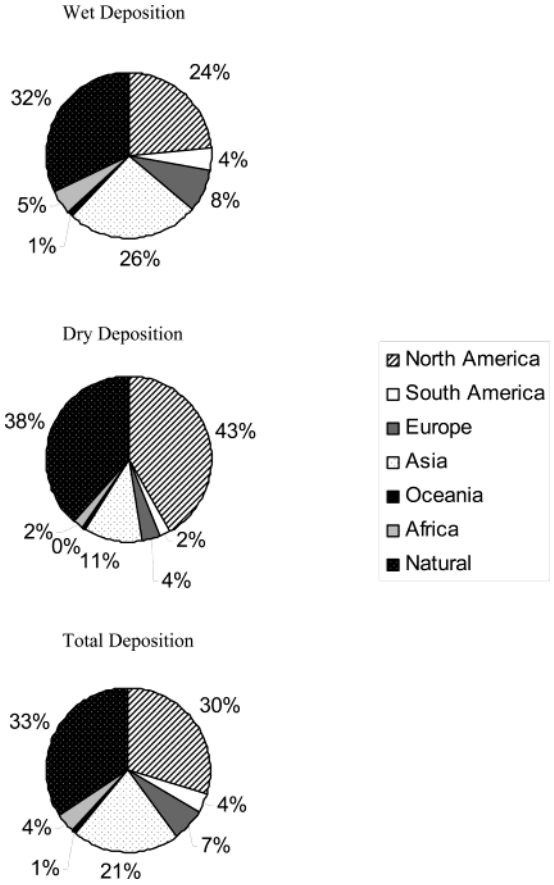

FIGURE 8. Relative contributions (%) of anthropogenic continental emissions and natural emissions from land and oceans to total mercury deposition over the contiguous United States for the base emission scenario.

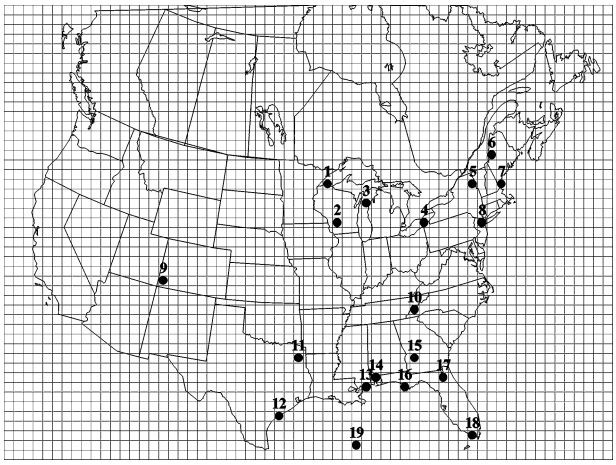

FIGURE 9. Locations of the receptor grid cells.

Refuge, NY (MDN site NY 20); Greenville Station, ME (MDN site ME09); New Castle, NH (MDN site NH05); Pines Lake, NJ; McPhee/Narraguinnep Reservoirs, CO [a total maximum daily load (TMDL) study site]; Great Smoky Mountains National Park; Longview, TX (MDN site TX21); upper Lavaca Bay, TX; Louisiana/Mississippi southern border; Mobile Bay, AL; Ichawahoa-chaway Lake, GA; Apalachicola Bay, FL; Lake Barco, FL; Everglades National Park, FL (MDN site FL11); and the Gulf of Mexico. Results for mercury deposition are presented in Figure 10.

At the reservoirs in southwestern Colorado, North American anthropogenic emissions contribute only 14%. The largest anthropogenic contribution comes from Asia with 27%.

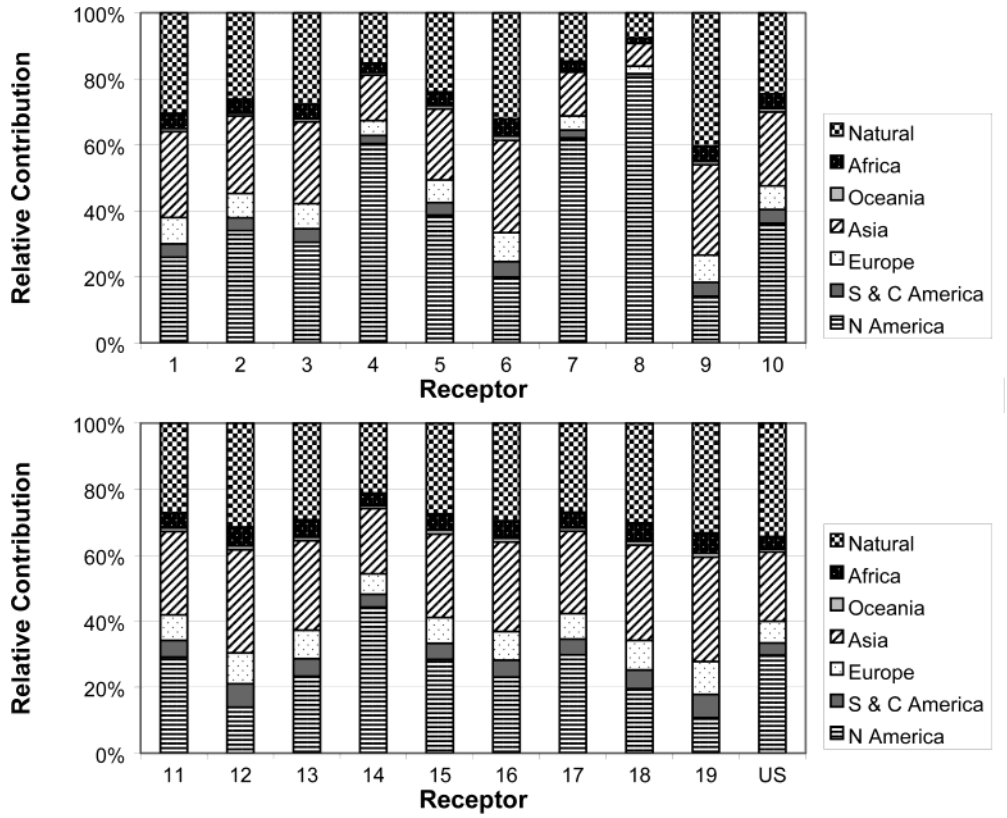

FIGURE 10. Relative contributions (%) of anthropogenic continental emissions and natural emissions to total mercury deposition at selected receptors for the base emission scenario.

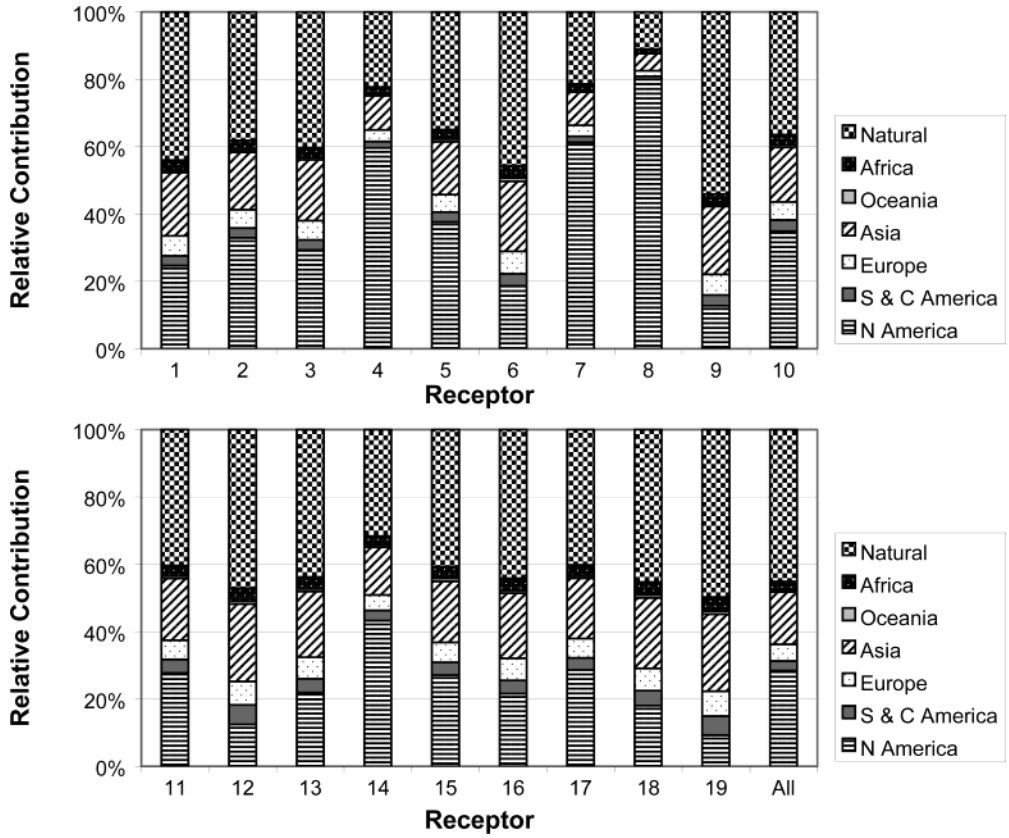

FIGURE 11. Relative contributions (%) of anthropogenic continental emissions and natural emissions to total mercury deposition at selected receptors for the lower bound emission scenario.

Natural emissions from land and the oceans account for 40%. In the Adirondacks, North American emissions account for the dominant fraction with 39% of total mercury deposition. Asian anthropogenic emissions still contribute signifi-

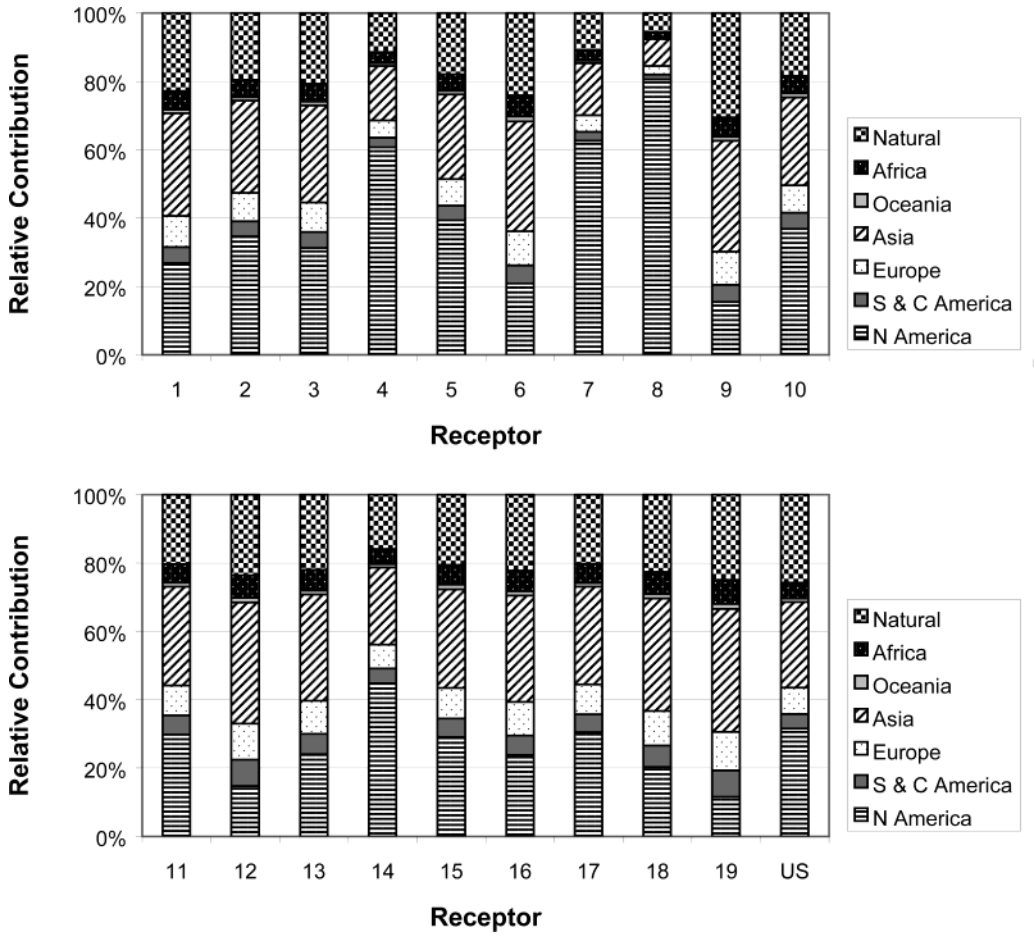

FIGURE 12. Relative contributions (%) of anthropogenic continental emissions and natural emissions to total mercury deposition at selected receptors for the upper bound emission scenario.

cantly with 22%; natural emissions account for 24%. At Devil's Lake, WI, North American anthropogenic emissions contribute 34% of mercury deposition with other global anthropogenic emissions contributing 40%; natural emissions contribute 26%. In the Everglades National Park, FL, North American emissions contribute only 20%. These results show a contribution from local and regional sources that is significantly less than previously estimated. For example, Dvonch et al. (*73*) used a receptor modeling approach with 1995 data from the Southern Florida Atmospheric Mercury Monitoring Study (SoFAMMS) to estimate that ~70% of mercury deposition in Florida originated from local sources in 1995. Guentzel et al. (*53*) used box model calculations based on 1992−1996 data from the Florida Atmospheric Mercury Study (FAMS) to estimate that 30−46% of mercury deposition may originate from local anthropogenic sources and the remainder from the global background. Our results show a much greater contribution from the global background and suggest that Asia (29% contribution) rather than Europe (9% contribution) provides the dominant contribution. This can be explained by the fact that Asian emissions are greater than European emissions by about a factor of 3.5.

At the other 15 receptors, the contribution of anthropogenic emissions from North America to total mercury deposition ranges from 11% (Gulf of Mexico) to 80% (Pines Lake, NJ). Contributions from Asian anthropogenic emissions range from 7% (Pines Lake, NJ) to 32% (Gulf of Mexico). Natural emissions contribute between 8% (Pines Lake, NJ) and 40% (McPhee/Narraguinnep Reservoirs, CO).

Results from the lower bound and upper bound emission scenarios are presented in Figures 11 and 12, respectively. For the lower bound scenario, the contribution of anthropogenic emissions from North America to total mercury deposition ranges from 9% (Gulf of Mexico) to 80% (Pines Lake, NJ). Contributions from Asian anthropogenic emissions range from 5% (Pines Lake, NJ) to 23% (Gulf of Mexico and upper Lavaca Bay, TX). Natural emissions contribute between 11% (Pines Lake, NJ) and 59% (McPhee/Narraguinnep Reservoirs, CO). For the upper bound scenario, the contribution of anthropogenic emissions from North America to total mercury deposition ranges from 12% (Gulf of Mexico) to 81% (Pines Lake, NJ). Contributions from Asian anthropogenic emissions range from 8% (Pines Lake, NJ) to 36% (Gulf of Mexico). Natural emissions contribute between 6% (Pines Lake, NJ) and 31% (McPhee/Narraguinnep Reservoirs, CO).

Current models of the atmospheric fate and transport of mercury may overestimate the local and regional impacts of some anthropogenic emission sources (*72*). Therefore, the calculated contributions of anthropogenic North American emissions are likely to represent upper bounds of actual contributions.

Acknowledgments

This work was conducted under funding from EPRI. We thank Dr. Leonard Levin, EPRI Project Manager, for his continuous support and constructive comments on this work. We also thank three reviewers for providing constructive comments that helped to clarify the presentation of the mercury global budget as well as the results of the simulations.

Supporting Information Available

Calculation of global Hg emissions budgets. This material is available free of charge via the Internet at http://pubs.acs.org.

Literature Cited

(1) Seigneur, C.; Karamchandani, P.; Lohman, K.; Vijayaraghavan, K.; Shia, R.-L. *J. Geophys. Res.* **2001**, *106*, 27795−27809.
(2) Pai, P.; Karamchandani, P.; Seigneur, C.; Allan, M. *J. Geophys. Res.* **1999**, *104*, 13855−13868.
(3) Seigneur, C.; Lohman, K.; Vijayaraghavan, K.; Shia, R.-L. *Environ. Pollut.* **2003**, *123*, 365−373.
(4) Seigneur, C.; Wrobel, J.; Constantinou, E. *Environ. Sci. Technol.* **1994**, *28*, 1589−1597.
(5) Shia, R. L.; Seigneur, C.; Pai, P.; Ko, M.; Sze, N. D. *J. Geophys. Res.* **1999**, *104*, 23747−23760.
(6) Ryaboshapko, A.; Bullock, R.; Ebinghaus, R.; Ilyin, I.; Lohman, K.; Munthe, J.; Petersen, G.; Seigneur, C.; Wängberg, I. *Atmos. Environ.* **2002**, *36*, 3881−3898.
(7) Sommar, J.; Gårdfeldt, K.; Strömberg, D.; Feng, X. *Atmos. Environ.* **2001**, *35*, 3049−3054.
(8) van Loon, L. L.; Mader, E. A.; Scott, S. L. *J. Phys. Chem. A* **2001**, *105*, 3190−3195.
(9) Ariya, P. A.; Khalizov, A.; Gidas, A. *J. Phys. Chem. A* **2002**, *106*, 7310−7320.
(10) Schroeder, W. H.; Munthe, J. *Atmos. Environ.* **1998**, *32*, 809−822.
(11) Pleijel, K.; Munthe, J. *Atmos. Environ.* **1995**, *29*, 1441−1457.
(12) Hedgecock, I. M.; Pirrone, N. *Atmos. Environ.* **2001**, *35*, 3055−3062.
(13) Graedel, T. E.; Keene, W. E. *Global Biogeochem. Cycles* **1995**, *9*, 47−77.
(14) Hansen, J.; Russel, G.; Rind, D.; Stone, P.; Lacis, A.; Lebedeff, S.; Ruedy, R.; Travis, L. *Mon. Weather Rev.* **1983**, *111*, 609−662.
(15) Seinfeld, J. H. *Atmospheric Chemistry and Physics of Air Pollution*; Wiley: New York, 1996.
(16) Seigneur, C.; Lohman, K.; Pai, P.; Heim, K.; Mitchell, D.; Levin, L. *Water Air Soil Pollut.* **1999**, *112*, 151−162.
(17) Lindberg, S. E.; Stratton, W. J. *Environ. Sci. Technol.* **1998**, *32*, 49−57.
(18) Xu, X.; Yang, X.; Miller, D. R.; Helble, J. J.; Carley, R. J. *Atmos. Environ.* **1999**, *33*, 4345−4355.
(19) Hanson, P. J.; Lindberg, S. E.; Tabberer, T. A.; Owens, J. G.; Kim, K.-H. *Water Air Soil Pollut.* **1995**, *80*, 373−382.
(20) Seinfeld, J. H.; Pandis, S. N. *Atmospheric Chemistry and Physics*; Wiley: New York, 1998.
(21) Pai, P.; Karamchandani, P.; Seigneur, C. *Atmos. Environ.* **1997**, *31*, 2717−2732.
(22) Leonard Levin, private communication, EPRI, Palo Alto, CA.
(23) Environment Canada. *Inventory of Anthropogenic Sources of Mercury in Atlantic Canada*; EPS-5-AR-98-1; Environmental Protection Branch: Downsview, ON, Canada, 1998.
(24) U.S. Department of Energy, http://www.fe.doe.gov/international/mexiover.html, 2000.
(25) Pai, P.; Niemi, D.; Powers, B. *Fuel Process. Technol.* **2000**, *65*−*66*, 101−115.
(26) U.S. Environmental Protection Agency. *Locating and Estimating Air Emissions from Sources of Mercury and Mercury Compounds*; EPA-454/R-97-012; Office of Air Quality Planning and Standards: Research Triangle Park, NC, 1997.
(27) Integrated Waste Services Association (IWSA); *The 1999 IWSA Waste-to-Energy Directory of United States Plants*; Washington, DC, 1999.
(28) U.S. Environmental Protection Agency. *Mercury Study Report to Congress, Vol. 3, Fate and Transport of Mercury in the Environment*; EPA-452/R-97-005; Washington, DC, 1997.
(29) U.S. Environmental Protection Agency. Toxics Release Inventory, http://www.epa.gov.tri.
(30) Canadian National Pollutant Release Inventory (NPRI), http://www.ec.gc.ca/pdb/npri, 1999.
(31) U.S. Environmental Protection Agency. National Emission Inventory(NEI),http://www.epa.gov/tth/chief/net/1999inventory.html, 2003.
(32) Gustin, M. S., et al. *J. Geophys. Res.* **1999**, *104*, 21831−21844.
(33) Zehner, R. E.; Gustin, M. S. *Environ. Sci. Technol.* **2002**, *36*, 4039−4045.
(34) University of North Dakota. Update on current volcanic activity, 2002, http://volcano.und.edu/vwdocs/current_volcs/current.html.
(35) Global Volcanism Program, Department of Mineral Sciences, Smithsonian Institution, Washington, DC, accessed June 2003, http://www.volcano.si.edu/gvp/reports/bulletin/index.cfm.
(36) Nriagu, J.; Becker, C. *Sci. Total Environ.* **2003**, *304*, 3−12.
(37) Mason, R. P.; Sheu, G.-R. *Global Biogeochem. Cycles* **2002**, *16*, DOI 10.1029/2001GB001440.
(38) Friedli, H. R.; Radke, L. F.; Lu, J. Y.; Banic, C. M.; Leaitch, W. R.; MacPherson, J. I. *Atmos. Environ.* **2003**, *37*, 253−267.
(39) Friedli, H. R.; Radke, L. F.; Prescott, R.; Hobbs, P. V.; Sinha, P. *Global Biogeochem. Cycles* **2003**, *17*, DOI 10.1029/2002GB001972.
(40) Lindqvist, O.; Johansson, K.; Åstrup, M.; Andersson, A.; Bringmark, L.; Hovsenius, G.; Iverfeldt, Å.; Mieli, M.; Timm, B. *Water Air Soil Pollut.* **1991**, *55*, i-261.
(41) Porcella, D. B. 1996. Inventory of North American Hg emissions to the atmosphere: relationship to the global mercury cycle. In *Global and Regional Mercury Cycles: Sources, Fluxes, and Mass Balances*; Baeyens, W., et al., Eds.; Kluwer Academic Publishers: Dordrecht, The Netherlands, 1996; pp 179−190.
(42) Lamborg, C. H.; Fitzgerald, W. F.; Damman, A. W. H.; Benoit, J. M.; Balcom, P. M.; Engstrom, D. R. *Global Biogeochem. Cycles*, **2002**, *16*, DOI 10.1029/2001GB001847.
(43) Schuster, P. F.; Krabbenhoft, D. P.; Naftz, D. L.; Dewayne Cecil, L.; Olson, M. L.; Dewild, J. F.; Susong, D. D.; Green, J. R.; Abbott, M. L. *Environ. Sci. Technol.* **2002**, *36*, 2303−2310.
(44) Bindler, R. *Environ. Sci. Technol.* **2003**, *37*, 40−46.
(45) Roos-Barraclough, F.; Shotyk, W. *Environ. Sci. Technol.* **2003**, *37*, 235−244.
(46) Gustin, M. S. *Sci. Total Environ.* **2003**, *304*, 153−167.
(47) Hintelmann, H.; Harris, R.; Heyes, A.; Hurley, J. P.; Kelly, C. A.; Krabbenhoft, D. P.; Lindberg, S.; Rudd, J. W. M.; Scott, K. J.; St. Louis, V. L. *Environ. Sci. Technol.* **2002**, *36*, 5034−5040.
(48) Landis, M. S.; Keeler, G. J. *Environ. Sci. Technol.* **2002**, *36*, 4518−4524.
(49) Bergan, T.; Gallardo, L.; Rohde, H. *Atmos. Environ.* **1999**, *33*, 1575−1585.
(50) Weiss-Penzias, P.; Jaffe, D. A.; McClintick, A.; Prestbo, E. M.; Landis, M. S. *Environ. Sci. Technol.* **2003**, *37*, 3755−3763.
(51) Sheu, G.-R.; Mason, R. P. *Environ. Sci. Technol.* **2001**, *35*, 1209−1216.
(52) Malcom, E. G.; Keeler, G. J. *Environ. Sci. Technol.* **2002**, *36*, 2815−2821.
(53) Guentzel, J. L.; Landing, W. M.; Gill, G. A.; Pollman, C. D. *Environ. Sci. Technol.* **2001**, *35*, 863−873.
(54) Landis, M. S.; Stevens, R. K.; Schaedlich, F.; Prestbo, E. M. *Environ. Sci. Technol.* **2002**, *36*, 3000−3009.
(55) Malcolm, E. G.; Keeler, G. J.; Landis, M. S. *J. Geophys. Res.* **2003**, DOI 10.1029/2002JD003084.
(56) Kellerhals, M., et al. *Atmos. Environ.* **2003**, *37*, 1003−1011.
(57) Poissant, L. *Sci. Total Environ.* **2000**, *259*, 191−201.
(58) Ebinghaus, R.; Kock, H. H.; Coggins, A. M.; Spain, T. G.; Jennings, S. G.; Temme, Ch. *Atmos. Environ.* **2002**, *36*, 5267−5276.
(59) Slemr, F.; Scheel, H. E. *Atmos. Environ.* **1998**, *32*, 845−853.
(60) Hladikova, V.; Petrik, J.; Jursa, S.; Ursinyova, M.; Kocan, A. *Chemosphere* **2001**, *45*, 801−806.
(61) Munthe, J., et al. *Atmos. Environ.* **2001**, *35*, 3007−3017.
(62) Wängberg, I., et al. *Atmos. Environ.* **2001**, *35*, 3019−3025.
(63) Kim, K.-H.; Kim, M.-Y.; Kim, J.; Lee, G. *Atmos. Environ.* **2002**, *36*, 3413−3427.
(64) Kim, K.-H.; Kim, M.-Y. *Atmos. Environ.* **2001**, *35*, 49−59.
(65) Tomiyasu, T.; Nagano, A.; Sakamoto, H.; Yonehara, N. *Sci. Total Environ.* **2000**, *259*, 231−237.
(66) Liu, S.; Nadim, F.; Perkins, C.; Carley, R. J.; Hoag, G. E.; Lin, Y.; Chen, L. *Chemosphere* **2002**, *48*, 97−107.
(67) Fang, F.; Wang, Q.; Liu, R.; Ma, Z.; Hao, Q. *Atmos. Environ.* **2001**, *35*, 4265−4272.
(68) Fostier, A.-H.; Forti, M. C.; Guimaraes, J. R. D.; Melfi, A. J.; Boulet, R.; Espirito Santo, C. M.; Hrug, F. J. *Sci. Total Environ.* **2000**, *260*, 201−211.
(69) Baker, P. G. L.; Brumke, E.-G.; Slemr, F.; Crouch, A. M. *Atmos. Environ.* **2002**, *36*, 2459−2465.
(70) Temme, C.; Slemr, F.; Ebinghaus, R.; Einax, J. W. *Atmos. Environ.* **2003**, *37*, 1889−1897.
(71) Mason, R. P.; Lawson, N. M.; Sheu, G. R. *Atmos. Environ.* **2000**, *34*, 1691−1701.
(72) Seigneur, C.; Karamchandani, P.; Vijayaraghavan, K.; Shia, R.-L; Levin, L. *Sci. Total Environ.* **2003**, *304*, 73−81.
(73) Dvonch, J. T.; Graney, J. R.; Keeler, G. I.; Stevens, R. K. *Environ. Sci. Technol.* **1999**, *33*, 4522−4527.

Received for review February 6, 2003. Revised manuscript received October 17, 2003. Accepted October 27, 2003.

ES034109T